

## ON LITHOSPHERIC FLEXURE SEAWARD OF THE BONIN AND MARIANA TRENCHES

J.H. BODINE and A.B. WATTS

*Lamont-Doherty Geological Observatory and Department of Geological Sciences of Columbia University,  
Palisades, NY 10964 (U.S.A.)*

Received September 29, 1978

Revised version received January 10, 1979

More than 25 bathymetry profiles have been used to examine the flexure of the Pacific lithosphere seaward of the Izu-Bonin and Mariana trenches. Selected bathymetry profiles have been corrected for the effects of sediment loading and compared to simple elastic and elastic-plastic models for lithospheric flexure seaward of these trenches. Profiles of the northern Mariana trench, where the seaward wall is relatively gentle, can be explained by a simple elastic model without an applied horizontal load. Profiles of the Izu-Bonin and southern Mariana trenches, where the seaward wall is relatively steep, can be explained by an elastic-plastic model with an applied load of 4.0–6.0 kbar, depending on the uniform yield stress assumed. If it is assumed the yield stress varies with depth the horizontal load required is significantly reduced ( $\leq 2.5$  kbar). The magnitude of the horizontal load cannot be determined with certainty, however, since it is not known how the yield stress may vary with depth. The elastic-plastic models examined all required significant differences ( $\sim 1.0$  kbar) in the horizontal load along the Izu-Bonin and Mariana trenches. These differences, which reach a maximum between the northern Izu-Bonin and northern Mariana trenches, appear to correlate with changes in the pattern of seismicity and tectonics landward of these trenches.

## 1. Introduction

The theory of plate tectonics is based on the concept of a strong rigid lithosphere which overlies a weak asthenosphere [1]. Studies have now been made of the deformation of the lithosphere caused by seamounts and sediments [2–5]. These studies show that the interiors of lithospheric plates respond to long-term ( $>10^6$  years) loads as a thin elastic layer overlying a weak fluid. There has been much recent interest in how the oceanic lithosphere responds as it approaches an island arc–trench system. It is now generally considered that trenches originate by downbending of the oceanic plate. However, unlike for the interiors of the plates, the downbending is not associated with an obvious surface load.

An important feature of island arc–trench systems

is a broad rise in topography, known as the Outer Rise, which occurs seaward of most deep-sea trenches [4,6,7]. Watts and Talwani [7] have shown there is generally a good correlation between the Outer Rise and a broad belt of positive free-air gravity anomalies. This correlation has been explained by an uncompensated warping of the oceanic lithosphere. Geological evidence show that although most Pacific Islands subside through time, Niue, Daito, and the Caroline islands have been uplifted [8]. Each of these islands are located within a few hundred kilometers of a trench axis. Recently Dubois et al. [9] have documented the uplift history of New Caledonia and shown that it is consistent with an upward flexure of the Australian plate as it approaches the New Hebrides trench.

The first recognition of the significance of the Outer Rise as a flexural feature was by Walcott [4] who postulated that it was analogous to the peripheral bulge around the Hawaiian seamounts and the Lauren-

tide ice sheet. Walcott [4] estimated the effective flexural rigidity of the Pacific plate at the Kuril trench as  $2 \times 10^{30}$  dyn-cm, on the basis of the amplitude and wavelength of the Hokkaido Rise.

Hanks [6] and Watts and Talwani [7] compared observed bathymetry and gravity profiles seaward of trenches to computed profiles based on a simple elastic model. They assumed an effective flexural rigidity for the Pacific plate of  $1.7 \times 10^{30}$  dyne-cm and suggested that the observed profiles could be best explained with an elastic model which included a large (5–10 kbar) horizontal compressive stress applied at the trench axis.

Parsons and Molnar [10] used a similar elastic model and showed that these large compressive stresses could be reduced if the bending moment was not constrained to be zero at the trench axis. They attributed the bending moment in a general way to the negative buoyancy of the dense downgoing slab.

Caldwell et al. [11] also used an elastic model and concluded that a large compressive stress was not required. They determined a value of  $5 \times 10^{29}$  dyne-cm for the effective flexural rigidity of the Pacific plate at the Kuril trench where the seaward wall is relatively steep and the Outer Rise is well developed. This value is about a factor of 3 to 4 smaller than that estimated by Walcott [4] and used by Hanks [6] and Watts and Talwani [7].

That viscous forces may be important in supporting the Outer Rise was considered by De Bremaecker [12] who used a viscous model for the oceanic plate and showed that computed profiles were similar in amplitude and wavelength to observed profiles. The main problem with his model is that he assumed an effective viscosity of  $10^{24}$  P, which corresponds to a relaxation time constant of  $10^5$  years. This value for the time constant will not explain gravity and bathymetry data over old loads ( $>5 \times 10^7$  years), such as the Emperor seamounts [5,13]. Furthermore, there is no evidence that the amplitude of the Outer Rise depends on the rate of subduction as required by the viscous model.

McKenzie [14] recently questioned the explanation of the Outer Rise as being due only to elastic or viscoelastic forces originating within the lithosphere and suggested that the Outer Rise may be a result of viscous flow beneath the plates. Although the ratio of the gravity anomalies to the bathymetry of the Outer

Rise is consistent with numerical experiments using a variety of models [14], it is not yet possible to determine the contribution of viscous forces to the observed flexure. Viscous forces and their associated stress concentrations may contribute to the bending moment applied to the subducting lithosphere.

These previous studies [6,7,10–12] are all limited in their application to the lithosphere because the elastic or viscous layer is assumed to be rheologically homogeneous. A number of recent attempts have been made to develop models for the rheology of the lithosphere based on the results of experimental rock mechanics [15–18].

That rocks which are relatively strong and yield by fracture near the Earth's surface may deform by flow under appropriate confining pressures and temperatures, has now been demonstrated [19–24]. A major difficulty in applying these experimental results to the upper mantle, however, is in extrapolating high experimental strain rates ( $\geq 10^{-8}$ /s) to more plausible rates ( $\leq 10^{-14}$ /s) for the lithosphere (for example, Stocker and Ashby [21]). Furthermore, it is difficult to apply experimental results based on single crystals to the more complicated compositions and varied grain sizes that may exist in the mantle. Although it is clear that, in general, the yield strength and ductility of upper mantle materials are pressure and temperature dependent, the specific relationship between these parameters is not yet well known.

An attempt to model deformation of the lithosphere at a trench using a more complex rheology has been made by Turcotte et al. [25] and McAdoo et al. [26]. They proposed an elastic-plastic model in which the oceanic lithosphere responds elastically to an applied load until a yield stress criteria is met. For bending stresses greater than the yield stress, some portions of the plate deform as a perfectly plastic material, capable of sustaining stresses only up to the yield stress. This model does not produce bending stresses as large as in the elastic model. In contrast to the elastic model [11], the elastic-plastic model is very sensitive to horizontal loading. Turcotte et al. [25] suggested that a horizontal compressive stress of up to 5.0 kbar was required to explain the Outer Rise seaward of the Kuril trench. This conclusion differs from the earlier result of Hanks [6] only in that a smaller horizontal stress is required.

The purpose of this paper is to examine, in detail,

flexure of the oceanic lithosphere seaward of a single island arc–trench system in the Pacific Ocean. We will assume that the Outer Rise, seaward of trenches, is a flexural feature and arises from elastic forces in the plate. We will compare bathymetry profiles corrected for sediment loading to computed profiles based on simple elastic and elastic-plastic models. The Izu-Bonin–Mariana trench system has been selected for three main reasons: (1) extensive bathymetry and seismic reflection profiles of the trench system are now available, most of which were satellite navigated; (2) the age of the approaching Pacific plate is greater than about 130 m.y. and thus the effect of cooling of the lithosphere on the depth of the sea floor is small; and (3) previous studies [7] have indicated there may be significant variations in the amplitude and shape of the Outer Rise seaward of this trench system. A major difference between this paper and previous studies is that we assume a relationship between crustal age and effective flexural rigidity (or effective elastic thickness) based on the results of seamount loading studies of the interior of the Pacific plate [13]. We use this relationship to better constrain both the boundary loads and the long-term mechanical properties associated with the Pacific lithospheric plate.

## 2. Analysis of data

We have examined more than 25 bathymetry profiles of the Izu-Bonin–Mariana island arc–trench system (Fig. 1). These data were obtained by Lamont-Doherty Geological Observatory, Hawaii Institute of Geophysics, Scripps Institution of Oceanography and National Oceanic and Atmospheric Administration (NOAA) research vessels. The bathymetry profiles, which were projected normal to the local trend of the trench (Fig. 2), show there are significant changes in the Outer Rise and seaward wall of the trench seaward of the Izu-Bonin and Mariana trenches. The Outer Rise is well defined seaward of the northern Izu-Bonin (profiles IB1 to IB9) and southern Mariana trenches (profiles MA10 to MA13) but poorly developed seaward of the southern Bonin (profiles IB11 to IB14) and northern Mariana (profiles MA1 to MA9) trenches. On some profiles seaward of the southern Mariana trench the Outer Rise is obscured by short-wavelength

topographic features associated with the Mid-Pacific Mountains. The seaward wall is relatively steep ( $\geq 4^\circ$ ) seaward of the northern Izu-Bonin and southern Mariana trenches and relatively gentle ( $\leq 2^\circ$ ) seaward of the southern Bonin and northern Mariana trenches.

In order to compare the observed bathymetry profiles (Fig. 2) to simple models of flexure, it is necessary to correct them for the effects of age and sediment loading. Evidence from Deep Sea Drilling Project (DSDP) sites and magnetic lineations [27,28] suggest that the oceanic lithosphere approaching the Izu-Bonin and Mariana trenches is at least 130 m.y. old and that changes in bathymetry due to thermal cooling of the oceanic lithosphere are small. Single and multi-channel seismic reflection profiles and long-range sonobuoy refraction measurements [29,30] indicate an uneven sediment distribution seaward of the trenches. Our procedure for making sediment corrections was to use available seismic data to “backstrip” the sediments and determine the depth the sea floor would have without the sediment load. We used the simple Airy model of unloading, and densities for the sediment were determined using velocities computed from sonobuoy measurements. In some cases the shape of the Outer Rise was considerably altered by removing the sediments from the observed bathymetry profiles.

For the purposes of model studies, we selected eight profiles for which the best seismic control was available and which best demonstrated the observed changes in the shape of the seaward wall of the trench and the Outer Rise (Fig. 2). The corrected bathymetry profiles were first compared with the elastic model to determine the effective flexural rigidity of the approaching Pacific plate. We found a large scatter in the estimates of effective flexural rigidity because of the difficulty of accurately determining the amplitude and wavelength of the Outer Rise. The range of effective flexural rigidity estimates from this comparison was from  $3 \times 10^{29}$  to  $1 \times 10^{31}$  dyn-cm, which corresponds to a range in the effective elastic plate thickness of 16–56 km.

It has recently been shown [13], on the basis of seamount loads on the interior of the Pacific plate, that the effective elastic thickness is related to crustal age and that it corresponds well to depths of oceanic isotherms based on the cooling plate model. Thus the effective elastic thickness of the west Pacific plate

seaward of the Izu-Bonin and Mariana trenches should be uniform and on the order of 40 km. By assuming this relationship between crustal age and effective elastic thickness, the difficulty of estimating the effective elastic thickness only from the shape of the Outer Rise is avoided (for example, Caldwell et al. [11]).

### 3. Simple models of flexure

We have compared the eight corrected bathymetry profiles of simple elastic and elastic-plastic models and now briefly outline the theoretical development of these models.

#### 3.1. Elastic model

The simple elastic model which we have used is similar to that applied by Hanks [6] and Watts and Talwani [7]. The main difference involves a modification of the boundary conditions and a reorientation of the origin [11,31]. In the elastic model the plate is acted upon by a restoring force,  $kw$ , given by  $gw(\rho_m - \rho_w)$ , where  $w$  is the deflection,  $g$  is average gravity, and  $\rho_m$  and  $\rho_w$  are defined in Table 1. If the applied loads comprise a vertical force,  $Q$ , a horizontal force,  $T$ , and a bending moment,  $M$ , the equilibrium equations are:

$$\frac{dT}{dx} = 0 \quad (1)$$

$$\frac{dQ}{dx} = -kw \quad (2)$$

$$\frac{dM}{dx} = -T \frac{dw}{dx} - Q \quad (3)$$

The relationship between the curvature of the plate and the bending moment is given by:

$$M = -D \frac{d^2w}{dx^2} \quad (4)$$

where  $D$  is the flexural rigidity of the elastic plate (Table 1). Equations (1) to (4) can be combined to give:

$$\frac{Dd^4w}{dx^4} - \frac{Td^2w}{dx^2} + kw = 0 \quad (5)$$

Following Caldwell et al. [11], the solution for the deflection  $w$  can be written:

$$w = w_0 \sin\left[\frac{x}{\alpha}(1 + \epsilon)^{1/2}\right] \exp\left[-\frac{x}{\alpha}(1 - \epsilon)^{1/2}\right] \quad (6)$$

where  $\alpha = (4D/k)^{1/4}$ ,  $\epsilon = -T/(4kD)^{1/2}$ , for boundary conditions:

$$x = 0, \quad w = 0$$

$$x = \infty, \quad w = 0$$

The parameter  $\epsilon$  is dependent on the magnitude of the horizontal loading and is proportional to the inverse square root of Young's Modulus,  $E$ . The value of  $\epsilon$  is small ( $\sim 0.1$ ) for the values of horizontal loading considered in this study ( $\leq 6$  kbar) and for reasonable variations in Young's Modulus. Thus  $\epsilon$  may be neglected in the elastic model [11]. If the shape of the Outer Rise is described by the location of its maximum value ( $x_b, w_b$ ) the deflection  $w$  is given by:

$$w = w_b \sqrt{2} \exp\left(\frac{\pi}{4}\right) \sin\left(\frac{x\pi}{4x_b}\right) \exp\left(\frac{-x\pi}{4x_b}\right) \quad (7)$$

where  $x_b$  is related to the effective elastic thickness,  $H$ , and Poisson's ratio,  $\nu$ , by:

$$x_b = \frac{\pi}{4} \left( \frac{EH^3}{3k(1 - \nu^2)} \right)^{1/4}$$

TABLE 1  
Summary of parameters used in computations

$w$ = deflection (cm)
$T_H$ = horizontal load (dyne/cm)
$E = 6.5 \times 10^{11}$ = Young's Modulus (dyne/cm <sup>2</sup> )
$k = 2.4 \times 10^3 = g(\rho_m - \rho_w)$ = resistance to vertical loading (dyne/cm <sup>3</sup> )
$\nu = 0.25$ = Poisson's ratio
$H$ = elastic thickness (cm)
$D = \frac{EH^3}{12(1 - \nu^2)}$ = rigidity (dyne-cm)
$\epsilon = -T_H/(4kD)^{1/2}$ = non-dimensional horizontal load
$\rho_w = 1.0$ density of water (g/cm <sup>3</sup> )
$\rho_m = 3.4$ = density of mantle (g/cm <sup>3</sup> )

3.2. Elastic-plastic model

The elastic-plastic model we have used is similar to that considered by Kachanov [32] and Prager and Hodge [33] and applied to trenches by McAdoo et al. [26]. In this model the plate behaves elastically until some yield criteria is met, beyond which parts of the plate deform as a perfectly plastic material with no strain hardening. For the assumption of plane strain and small vertical forces [33], the stress distribution in an elastic plate is the sum of the stresses due to horizontal loading and to bending (Fig. 3). This can be expressed as:

$$\sigma_x(y) = T/H + 12 My/H^3 \tag{8}$$

where  $-H/2 \leq y \leq H/2$ . The horizontal load and the bending moment are given by integrating over the

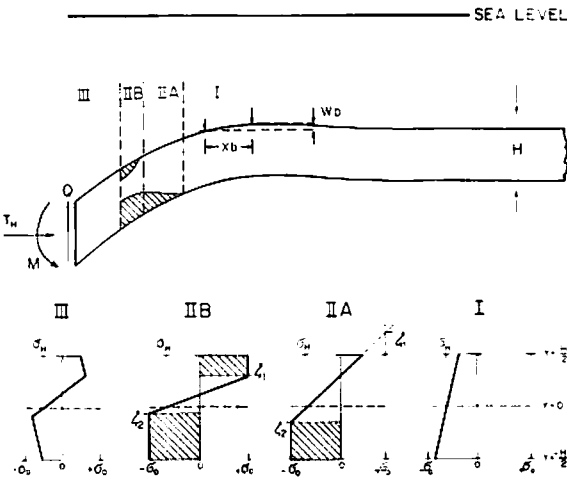


Fig. 3. A simple illustration of a flexing slab of elastic thickness  $H$ , and boundary loads  $Q$  (vertical load),  $T$  (horizontal load), and  $M$  (applied bending moment). The origin, from which  $x_b$  and  $w_b$  are measured to represent the position of the Outer Rise maximum, is the first point of zero deflection seaward of the trench. Four regions with distinct modes of deformation in the elastic-plastic model (I, IIA, IIB, III) are indicated with corresponding vertical cross sections of the stress profile. Hatched areas indicate plastic deformation. Region I: elastic model applies, no plastic deformation occurs. Region IIA: plastic yielding occurs on one side of the plate. Region IIB: plastic yielding occurs on both sides of the plate with an elastic "core" between. Region III: plate begins to unbend and all plastic yielding ceases. For the stress profiles, compression = -, tension = +.  $\xi_1$  and  $\xi_2$  represent the top and bottom, respectively, of the elastic region corresponding with flexural curvature as described in the Appendix.

vertical stress profile:

$$T = \int_{-H/2}^{H/2} \sigma_x(y) dy \tag{9}$$

$$M = \int_{-H/2}^{H/2} \sigma_x(y) y dy \tag{10}$$

Those parts of the plate which deform plastically (region IIA and IIB, Fig. 3) will not sustain stresses higher than the yield stress. Within these regions, the stress profile is no longer a smoothly varying function through the plate. Equation (10) shows that for this change in the stress profile, there is a departure from the simple relation between bending moment and curvature that exists in the purely elastic model (equation 4).

The differential expressions are solved by relating the curvature of the plate to the yield criteria and then numerically integrating. The detailed development for these steps is described in the Appendix.

4. Model results

We began by comparing the eight corrected bathymetry profiles to computed profiles based on the elastic model (Fig. 4). We used the relationship between crustal age and effective elastic thickness [13] to first estimate  $x_b$ , and the general topography of the Outer Rise to next estimate  $w_b$ . A "best fitting" curve was then obtained based on the elastic model.

Fig. 4 shows that only bathymetry profiles MA4 and MA9 of the northern Mariana trench can be explained by elastic models. The elastic model could not explain the steep slope seaward of the trench on profiles IB1, IB6 and IB9 of the northern Izu-Bonin trench or profiles MA12 and MA13 of the southern Mariana trench. A better fit to the seaward wall of the trench could only be obtained by increasing the applied bending moment. However, the bending moment determines  $w_b$  which we found could not be varied by a large enough amount and still explain the observed Outer Rise amplitude.

We then compared the corrected bathymetry profiles to curves derived from the elastic-plastic model. Deflection profiles for this model with no horizontal load applied were essentially indistinguishable from the elastic model results. Thus, only the six profiles

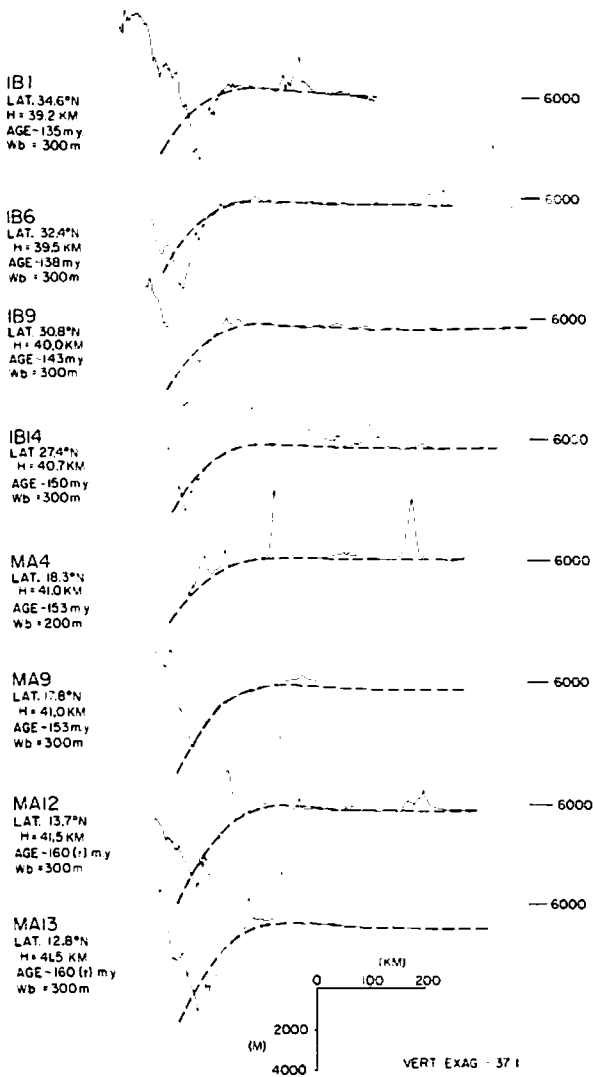


Fig. 4. Eight selected profiles corrected for sediment loading are compared to theoretical curves from the elastic model. The effective elastic thickness assumed for each profile is the depth to the 500°C isotherm calculated using a simple cooling plate model ( $T_1 = 500^\circ\text{C}$ ) [13],  $T_0 = 0^\circ\text{C}$ ,  $T_L = 1333^\circ\text{C}$ , plate thickness = 125 km, thermal time constant = 62.8 m.y.). With the constraint of an age dependence of the elastic thickness, only two of the eight profiles (MA4 and MA9) can be explained by purely elastic deformation.

not explained by the elastic model were further examined. We used the same assumed values for  $x_b$  and  $w_b$  as used in the elastic models (Fig. 4). The variables in this model are the applied horizontal load,  $\sigma_H$ , and the yield stress,  $\sigma_0$ . Since the shape of the

Outer Rise is determined by  $x_b$  and  $w_b$ , the match to observed profiles for the elastic-plastic model is based mainly on the slope of the seaward wall of the trench. We found that a number of combinations of yield stress and horizontal load could produce the required slopes. For each corrected profile a wide range of yield stress values were assumed and, for each value, the corresponding horizontal load was found.

The results are illustrated in Fig. 5 for "low" yield stress values ( $\sigma_0 = 3.3$  kbar) and "high" values ( $\sigma_0 = 6.0$  kbar). These values were chosen in order to illustrate how the model responds to different stress regimes. We were not able to consider a yield stress less than 3 kbar because the plate deformed entirely plastically. The horizontal load required to explain the observed profiles for "low" yield stress was in the range 0.2–0.6 kbars, and the load required for "high" yield stress was in the range 4.0–5.0 kbar. Profiles MA12 and MA13 of the southern Mariana trench could be equally well explained by results of both the "high" and "low" yield stress examples. However, profiles IB1, IB6, and IB9 of the northern Izu-Bonin trench, where the seaward wall is relatively steep, could be best explained by "high" rather than "low" yield stress values (Fig. 5).

The following conclusions can be derived from this comparison of the elastic and elastic-plastic models to the Izu-Bonin and Mariana trenches.

- (1) Profiles of the northern Mariana trench, where the seaward wall is relatively gentle, can be explained without an applied horizontal load. Profiles of the Izu-Bonin and southern Mariana trenches, however, where the seaward wall is relatively steep, require an applied horizontal load.
- (2) Although the horizontal load required increases as the yield stress assumed increases, the variation of the load required *along* the trench remained similar and on the order of several hundred bars.
- (3) The largest horizontal load was required for the northern Izu-Bonin trench.
- (4) The best overall fit to all trench profiles was obtained with the "high" rather than "low" yield stress models.

## 5. Discussion

In previous sections we have used a simple elastic-plastic rheology to deduce information about the

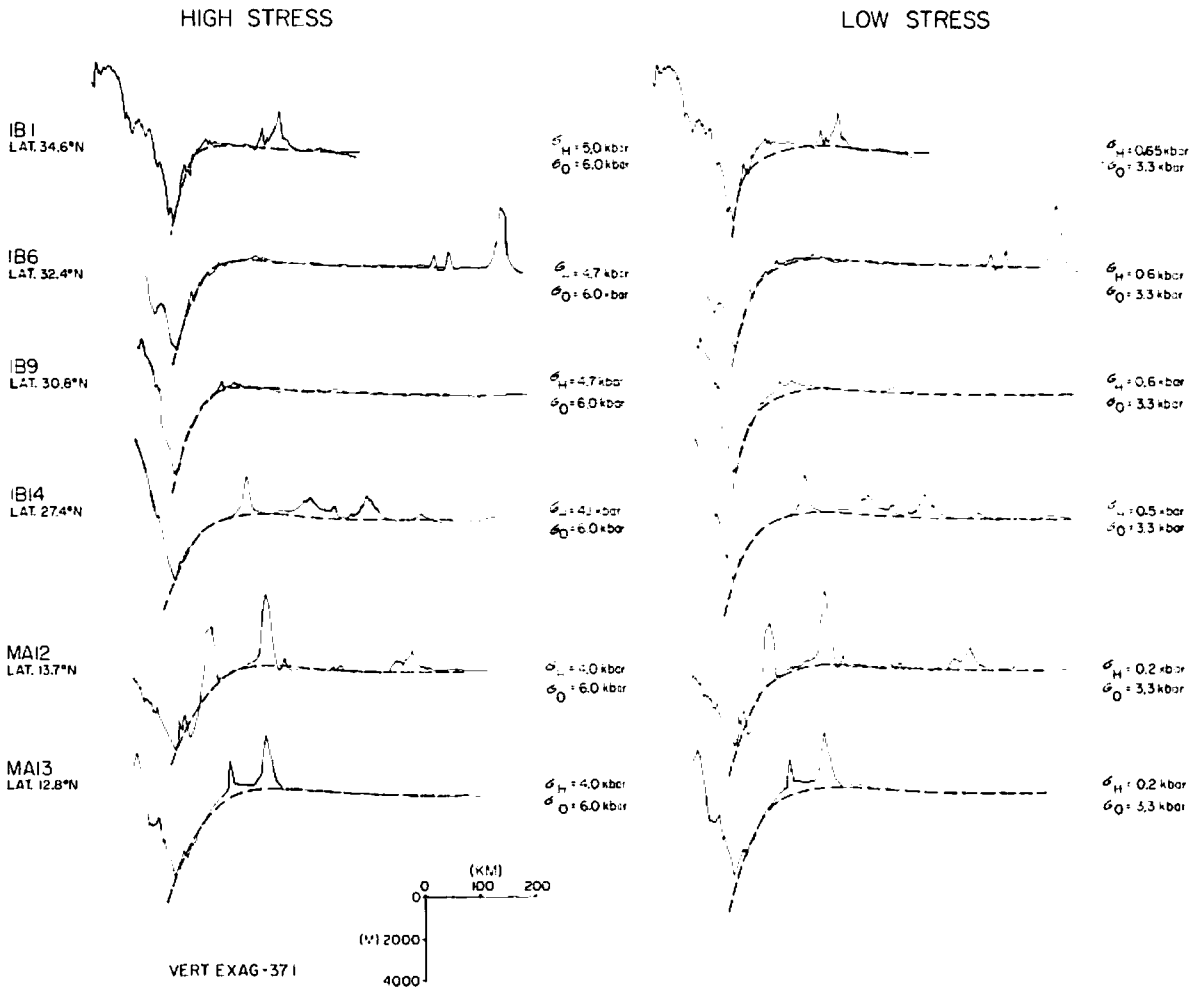


Fig. 5. Comparisons of observed profiles with theoretical curves of the elastic-plastic model.  $\sigma_0$  = yield stress,  $\sigma_H$  = horizontal load. Two examples, "high" stress ( $\sigma_H > 4.0$  kbar) and "low" stress ( $\sigma_H < 1.0$  kbar) are shown to demonstrate that a range of combinations of yield stress and horizontal loads can approximate the data. For each case the variation of  $\sigma_H$  along the trench is similar ( $< 1.0$  kbar). Note that where seaward trench walls are very steep, the "high" stress curves provide better fits.

boundary forces on the approaching Pacific plate. We concluded that models with large applied horizontal loads appear to give the best fit to the observed profiles. In this section we examine how variations in this simple rheology may affect this conclusion and how these variations may be better constrained by results from experimental rock mechanics.

In the "high"-stress model in Fig. 5 plastic yielding occurs more readily on one side of the plate than on the other. For the case of an applied horizontal compression (Fig. 3), the tensile stresses due to bending at

the top of the plate are reduced while the compressive stresses at the bottom are increased. This results in plastic yielding at the bottom of the plate "earlier" in the curvature with little or no yielding at the top. The wavelength of the deflection curve is therefore effectively shortened and a greater curvature develops. These changes in the flexure curve could also be achieved for lower applied horizontal loads with a yield stress which is depth dependent rather than uniform. For example, with an applied horizontal compression, a yield stress that *decreases* with depth

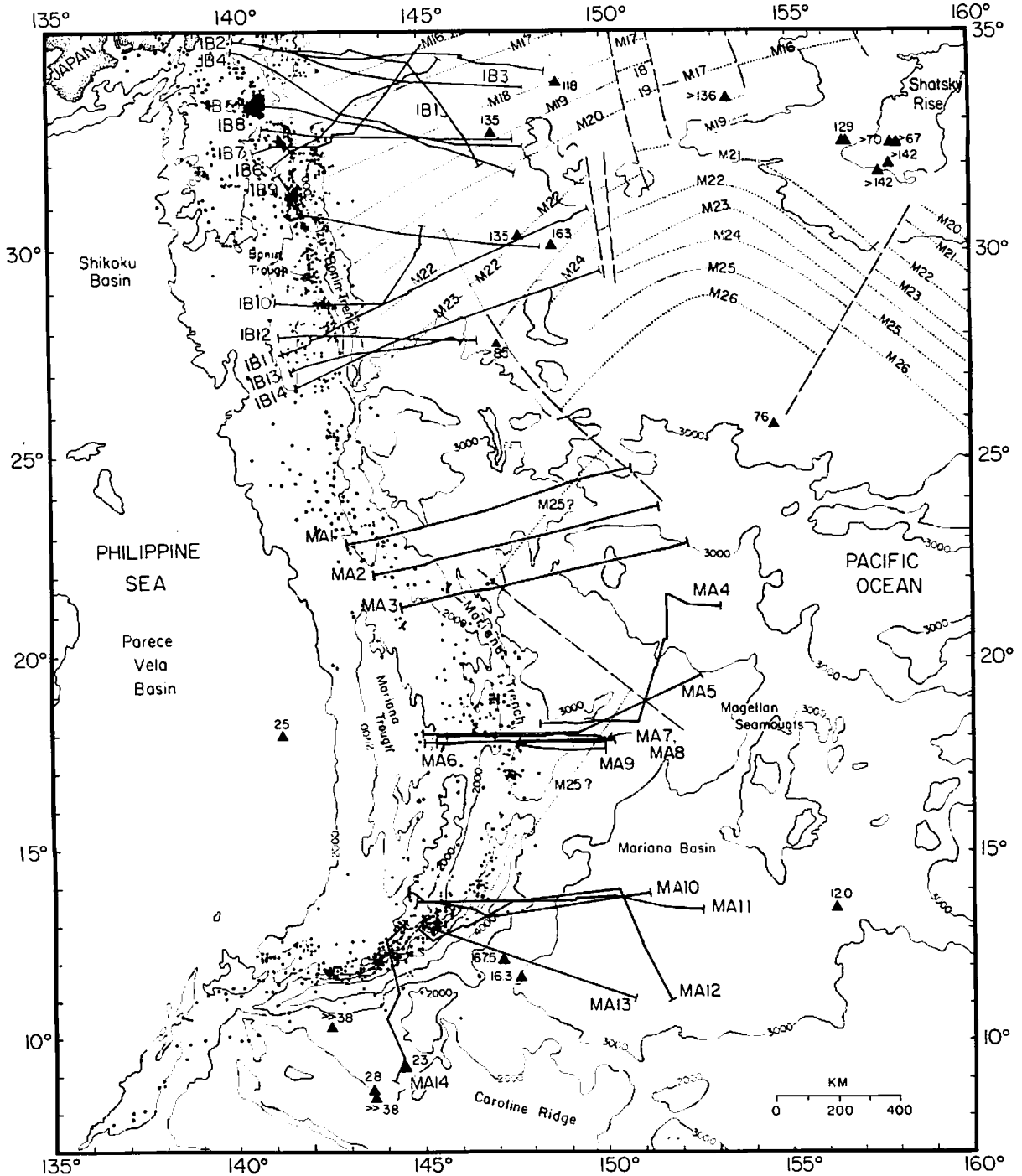


Fig. 1. Location of observed bathymetry profiles used in this study. Contours are at 1000-fathom intervals. Dotted lines are magnetic lineations from Hide et al. [27] and Hussong [28]. Black triangles are DSDP sites with associated age determinations in m.y. B.P. Darkened circles represent epicenter locations of shallow earthquakes (<100 km) since 1962.

IZU-BONIN TRENCH

MARIANA TRENCH

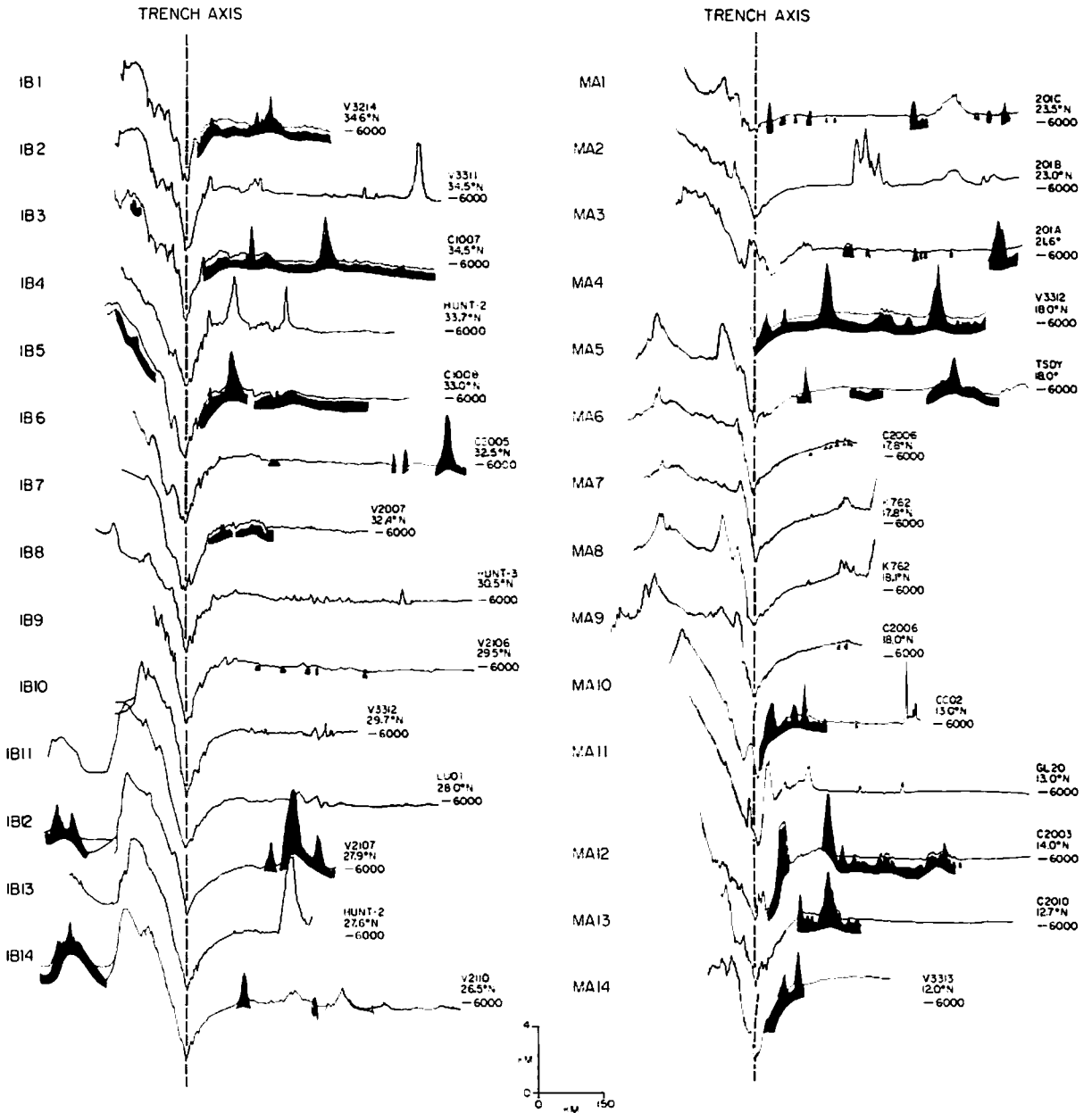


Fig. 2. Observed bathymetry profiles projected normal to the trench and plotted from west to east. Vertical exaggeration is 37 : 1. Stippled areas represent most well-defined basement from seismic reflection data. The 6000-m depth is indicated by a horizontal dashed line. Seismic refraction and multichannel seismic reflection data not illustrated in this figure were used to "offload" sediments from eight selected profiles.

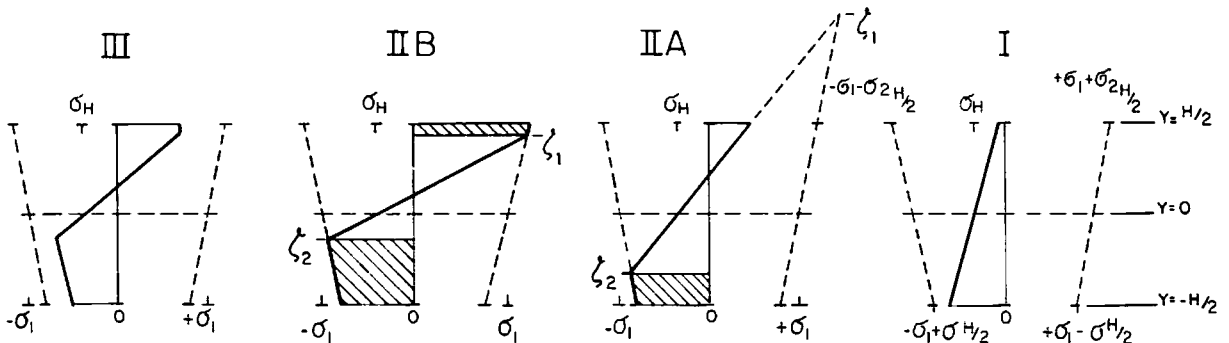


Fig. 6. Stress profiles for regions I-III for the elastic-plastic model with depth-dependent yield stress. For this diagram the horizontal load ( $\sigma_H$ ) is compressive (-) and yield stress is linearly decreasing with depth.  $\sigma_1$  = average yield stress;  $\sigma_2$  = yield stress gradient with depth.  $\xi_1$  and  $\xi_2$  are as in Fig. 3.

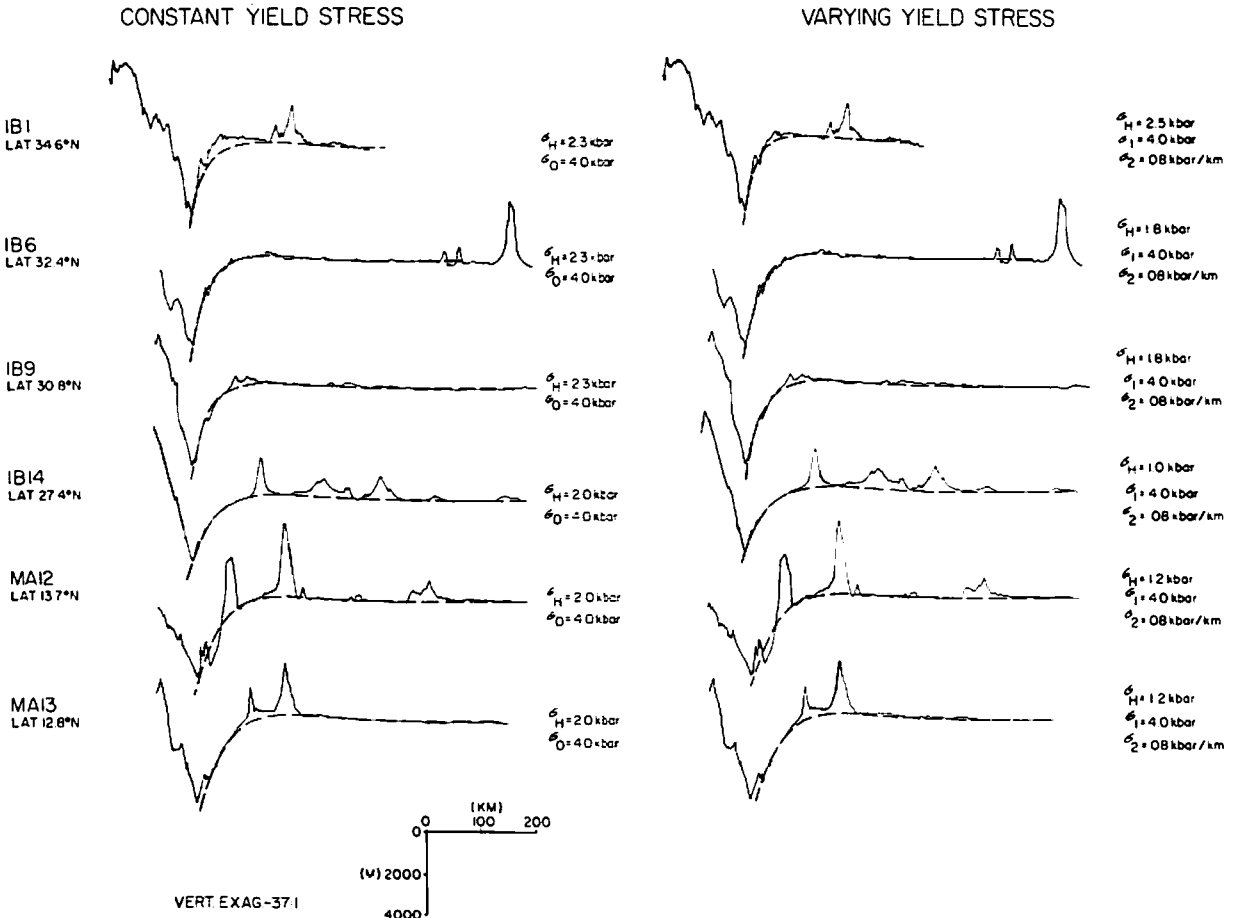


Fig. 7. Comparison of results of elastic-plastic model with uniform and depth-dependent yield stress. Since only relative differences between the results of the two models are significant, an average yield stress of 4.0 kbar is chosen to limit the yield stress at the top and bottom of the slab to "reasonable" values. This combination of  $\sigma_1$  and  $\sigma_2$  is equivalent to a linear decrease of yield stress from 5.6 kbar at the top of the plate to 2.4 kbar at the bottom. For all profiles except IB1, equally good approximations are provided by both models although, with a varying yield stress, significantly less horizontal loading is required (compression for this diagram). To obtain as good a fit to IB1 using a uniform yield stress, requires  $\sigma_0 > 6.0$  kbar and  $\sigma_H > 5.0$  kbar.

would yield easily in the bottom of the plate and perhaps not at all at the top.

To examine this effect, we modified the elastic-plastic model [26] to include a depth-dependent yield stress (Appendix). In this model the yield stress decreases linearly with depth. The corresponding stress profiles for compressive loading in each region of the deformed plate are shown in Fig. 6.

The results for the depth-dependent yield stress model are compared to the observed bathymetry profiles in Fig. 7. An average yield stress of 4.0 kbar was assumed for the comparison in this figure as an intermediate value of those used in Fig. 6. These comparisons show that for the most part, both models give equally good fits to the observed profiles. The main difference is that significantly smaller horizontal loads are required for the depth-dependent model (Fig. 7). We note that for profile IB1 (Fig. 7), there is a significantly better fit for the depth-dependent than for the uniform yield stress model. To provide an equally good fit for this profile the uniform yield stress model requires values for the yield stress and horizontal load of at least 6 and 5 kbar respectively. Fig. 7 shows that although the applied horizontal load is smaller, the variation in the required stress along the trench is similar for both models.

When using models in which the yield stress is constant with depth, similar stress distributions lead to similar deformations for both compressional and tensional horizontal loading. Whereas for compressional loading yielding occurs first at the bottom of the plate, when tension is applied yielding occurs first at the top. For the two cases, however, because of symmetry, the total stress distribution is the same. Therefore, differences in the resulting deformations, as a function of the total vertical stress distribution, are due only to the change in the sign of the second term in equation (5) and a "buckling effect" which develops for regional compression. For the applied loads considered in this study we could not distinguish between deformations caused by compressional or tensional horizontal loading.

The elastic-plastic model with a varying yield stress differs in that a given horizontal load can be combined with a yield stress that either increases or decreases with depth. The four possible combinations (tension with decreasing or increasing yield stress, compression with decreasing or increasing yield stress) result in

two different deflection curves. For identical parameters (except for sign), the combinations of compression and decreasing yield stress with depth, and tension and increasing yield stress produce the greater deflections and curvatures. Deformations resulting from these combinations are similar for the same reasons as described for a model with constant yield stress.

Without knowledge of which gradient of yield stress may more closely represent existing rheological variations, we have not been able to distinguish between effects of tensional and compressional regimes. With better constraints on the yield stress gradient, however, an estimation of which type of horizontal load might exist could be made.

We have used an elastic-plastic model in which we assumed compressional horizontal loading and a yield stress which decreases with depth. We have not taken into account, however, that the yield strength of upper mantle materials may be different under compression than tension. In each elastic-plastic model the yield strength is identical for both compression and tension. The effect of using a yield strength which is lower in tension than in compression is to subject the upper part of the plate to more extensive tensile yielding. Thus the horizontal loads required to explain the observed profiles in Fig. 7 would be reduced. Furthermore, we have not taken into account that the oceanic crust is most likely highly fractured and, at low confining pressure, should deform by frictional sliding (cataclastic deformation) [34]. The onset of frictional sliding is strongly dependent on pressure [35]. Thus the yield strength may be low near the surface of the plate and may increase with depth until temperature effects begin to predominate. With higher temperatures, thermally activated creep acts to diminish the magnitude of stresses that can be sustained by mantle materials and thus may effectively weaken the lower lithosphere [20,21,36].

Goetze [37] has developed a model using an elastic-plastic rheology for the lithosphere in which variations of the yield strength are constrained by data from experimental rock mechanics. He used this model to estimate the elastic thickness of the lithosphere required to explain the bending moments and deflections observed seaward of a trench. A main result of his study is that the elastic thickness obtained

for a profile of the Izu-Bonin Outer Rise is about 30% larger than the effective elastic thickness determined by Caldwell et al. [11] using a simple elastic model.

We would not expect that the *effective* elastic thickness determined from simple elastic models would correspond to the *actual* elastic thickness of the plate. The relation of the effective elastic thickness to crustal age suggests that the mechanical behavior of the lithosphere is controlled largely by temperature [13]. Although the effective elastic thickness may correspond to the depth of a particular oceanic isotherm, the actual depth to which materials behave elastically may be somewhat greater. The effect of inelastic processes occurring once the yield strength is exceeded is to limit the magnitude of the stresses which can be sustained. The materials which deform in this way will be weaker than those which deform only elastically and thus will be associated with a smaller estimate of elastic thickness.

These considerations suggest that the *effective* elastic thickness determined using elastic models is a minimum estimate for the depth to which materials behave elastically on long time scales. This would affect the results of this study in that the applied horizontal force required,  $T$ , is distributed over a greater depth, and the required applied horizontal stress,  $\sigma_{11}$ , would thus be reduced ( $\sigma_{11} = T/H$ ). We do not expect, however, that the changes in horizontal loading required along the trench would be significantly altered.

## 6. Tectonic implications

Using the elastic-plastic model with a varying yield stress we have determined that smaller horizontal stresses than those previously estimated exist across the Izu-Bonin island arc-trench system. For the models used in this study, variations in these stresses *along* the trench system are on the order of 1 kbar. The stresses are low across the northern Mariana trench, intermediate across the southern Bonin and southern Mariana trench and high across the northern Bonin trench. These variations in the stress distribution appear to correlate with changes in seismicity and tectonics along these trench systems.

A number of studies have now been carried out which have delineated the distribution of great earth-

quakes ( $M \geq 8.0$ ) and shallow seismicity along the Izu-Bonin-Mariana island arc-trench system [38–41]. Kelleher et al. [41] have shown that the region of rupture zones of great earthquakes and areas that are considered “most likely” to experience future great earthquakes extends south of Japan to about  $33.7^\circ\text{N}$ . This region includes profile IB1 (Fig. 7) which, in our models, requires the highest stress across the trench. Between  $33.7^\circ\text{N}$  and about  $26^\circ\text{N}$  there is no historical record of great earthquakes and the abundance of shallow seismicity decreases to the south (Fig. 1; [39]). This region includes profiles IB6, IB9 and IB14 which require intermediate values of stress across the trench (Fig. 7). The arc-trench system between about  $26^\circ\text{N}$  and  $14^\circ\text{N}$  is also characterized by an absence of great earthquakes but, in addition, is associated with a further decrease in the abundance of shallow seismicity (Fig. 1; [39]). This region includes profiles MA4 and MA9 which require the lowest stress across the trench. Fig. 1 shows that south of about  $14^\circ\text{N}$  there is a significant increase in the abundance of shallow seismic events. This region includes profiles MA12 and MA13 which require intermediate values of stress across the trench (Fig. 7). Although it is generally believed that great earthquakes have not occurred in this region there is a history of destructive seismic activity on Guam ( $13.5^\circ\text{N}$ ; [42]).

These observations suggest there may be a simple relationship between the stress distribution inferred from the mechanical behavior of the approaching Pacific plate and the pattern of seismicity in the adjacent island arc-trench system. Regions of smallest stress appear to be associated with less abundant shallow seismicity and an absence of great earthquakes, while regions of largest stress appear to be associated with abundant shallow seismicity and great earthquakes. Those regions for which intermediate stresses are inferred appear to be associated with moderate shallow seismicity and, possibly, the potential for destructive earthquakes.

Tectonic studies of the eastern Philippine Sea [43, 44] suggest active crustal extension may be occurring on or landward of the Izu-Bonin and Mariana island arcs. The most convincing evidence for active extension is in the Mariana trough which is believed to have formed by normal processes of sea-floor spreading at an axial rift valley [45]. The Mariana trough extends

from about 21.5°N to 14°N. Bathymetry profiles seaward of this region (for example, profiles MA4 and MA9, Fig. 4) do not require any horizontal load to explain the relatively gentle seaward wall of the trench, while profiles north and south of this region do require horizontal loads (Fig. 7). These observations suggest a correlation between regions of the arc which do not require horizontal loads and the presence of active crustal extension behind the arc.

These correlations of the stress regime, seismicity patterns and tectonics along the Izu-Bonin–Mariana island arc–trench system can be generally explained within the framework of the model proposed by Kanamori [40,46]. In this model, the degree of mechanical coupling (or decoupling) between convergent lithospheric plates varies along arc–trench systems. Regions of strong coupling are associated with great earthquakes, abundant seismicity and an absence of an extensional basin behind the island arc. Regions of decoupling are associated with an absence of great earthquakes, less abundant seismicity and the presence of an extensional basin. Kanamori [40] associates regions of strong coupling with compression and regions of decoupling with tension. For the Izu-Bonin–Mariana arc–trench system this model predicts a partial coupling to the north and decoupling to the south. These results are in good general agreement with the determinations of stress along the arc–trench system deduced in this study (Fig. 7).

Although the seaward wall of the northern Mariana trench could be explained in the absence of horizontal loads we found that small loads (compression or tension) could exist without significantly altering the computed profiles shown in Fig. 4. Thus tension such as suggested by Kanamori [40] could exist across the northern Mariana trench. The results of this study are, therefore, not in disagreement with a stress regime which varies from compression to tension and then compression along the arc–trench system.

The results of this study cannot be simply explained in terms of the model proposed by Kelleher and McCann [47]. In this model buoyant features on the approaching oceanic lithosphere resist or, in some cases, terminate subduction at a trench. We have found that the lowest stresses are required across the Mariana trench where the Marcus-Necker ridge and Magellan seamounts intersect the trench. The low stresses could arise because the Philippine Sea plate

is moving westward with respect to the Pacific plate at the Mariana trench. Alternatively, the Marcus-Necker ridge and Magellan seamounts may be regionally rather than locally compensated. For regional compensation these features would have relatively shallow crustal “roots” and would therefore probably be more easily subducted at the trench.

## 7. Conclusions

This detailed study of bathymetry profiles of the Izu-Bonin and Mariana trenches allows the following conclusions to be made.

(1) Bathymetry profiles show there are significant variations in the shape of the Outer Rise and the steepness of the seaward wall along the Izu-Bonin and Mariana trenches.

(2) These profiles, when corrected for sediments, can be compared to simple elastic and elastic-plastic models for lithospheric flexure seaward of trenches. By assuming a relationship between flexural rigidity (elastic thickness) and crustal age, information can be obtained on the boundary loads and the mechanical behavior of the approaching Pacific plate.

(3) Profiles of the northern Mariana trench, where the seaward wall is relatively gentle ( $\leq 2^\circ$ ), can be explained by a simple elastic or elastic-plastic model without an applied horizontal load. Profiles of the Izu-Bonin and southern Mariana trenches where the seaward wall is relatively steep ( $\leq 4^\circ$ ) can be explained with an elastic-plastic model by varying the horizontal load applied across different sections of the trench system.

(4) For the elastic-plastic model with a yield stress that is uniform with depth, the steep seaward walls can be best explained by applying relatively large horizontal loads ( $\sim 4\text{--}6$  kbar).

(5) The horizontal load required to explain these profiles is significantly reduced if it is assumed that the yield stress varies with depth. A yield stress that varies with depth is expected on the basis of results from experimental rock mechanics although specifically how it may vary is not yet known with certainty.

(6) With the present models, it is not possible to reliably determine either the magnitude of the horizontal stress or even whether the stress is compress-

sive or tensile. However, we prefer a model in which the stresses are relatively small ( $\leq 2.5$  kbar) and compressive.

(7) The changes in the horizontal load required along the Izu-Bonin and Mariana trenches appear to correlate with changes in the seismicity and tectonics of the adjacent island arcs. The larger horizontal loads inferred for the northern Bonin trench correlate with abundant shallow seismicity, great earthquakes ( $M > 8.0$ ), and an absence of active crustal extension landward of the trench. The absence of a horizontal load inferred for the northern Mariana trench correlates with relatively little shallow seismicity, an absence of great earthquakes and the presence of active crustal extension landward of the trench.

#### Acknowledgements

We are grateful to T. Chen, W. Haxby, J.R. Cochran, M.S. Steckler, and R. Kranz for critically reading the manuscript and to an anonymous reviewer for pointing out the potential importance of the buckling effect. D. Turcotte, B. Evans, and T. Chen provided preprints of papers prior to publication. This work was supported by the National Science Foundation grant IDO 75-16027.

#### References

- 1 J. Barrell, The strength of the Earth's crust, *J. Geol.* 22 (1914) 729.
- 2 F.A. Vening-Meinesz, Gravity over the Hawaiian archipelago and over the Madeira area: conclusions about the Earth's crust, *Proc. K. Ned. Akad. Wetensch.* 44 (1941) 1.
- 3 R. Gunn, A quantitative study of the lithosphere and gravity anomalies along the Atlantic Coast, *Franklin Inst. J.* 237 (1944) 139.
- 4 R.I. Walcott, Flexural rigidity, thickness, and viscosity of the lithosphere, *J. Geophys. Res.* 75 (1970) 3941.
- 5 A.B. Watts and J.R. Cochran, Gravity anomalies and flexure of the lithosphere along the Hawaiian-Emperor seamount chain, *Geophys. J.R. Astron. Soc.* 38 (1974) 119.
- 6 T.C. Hanks, The Kuril Trench-Hokkaido Rise system: large shallow earthquakes and simple models of deformation, *Geophys. J.R. Astron. Soc.* 23 (1971) 173.
- 7 A.B. Watts and M. Talwani, Gravity anomalies seaward of deep-sea trenches and their tectonic implications, *Geophys. J.R. Astron. Soc.* 36 (1974) 57.
- 8 J.T. Wilson, Pattern of uplifted islands in the main ocean basins, *Science* 139 (1963) 592.
- 9 J. Dubois, J. Launay and J. Recy, Some new evidence on lithospheric bulges close to island arcs, *Tectonophysics* 26 (1975) 189.
- 10 B. Parsons and P. Molnar, The origin of outer topographic rises associated with trenches, *Geophys. J.R. Astron. Soc.* 45 (1976) 707.
- 11 J.G. Caldwell, W.F. Haxby, D.E. Karig and D.L. Turcotte, On the applicability of a universal elastic trench profile, *Earth Planet. Sci. Lett.* 31 (1976) 239.
- 12 J.C. De Bremaecker, Is the oceanic lithosphere elastic or viscous? *J. Geophys. Res.* 82 (1977) 2001.
- 13 A.B. Watts, An analysis of isostasy in the world's oceans, 1. Hawaiian-Emperor seamount chain, *J. Geophys. Res.* 83 (1978) 5989.
- 14 D.P. McKenzie, Surface deformation, gravity anomalies and convection, *Geophys. J.R. Astron. Soc.* 48 (1977) 211.
- 15 H.J. Neugebauer and G. Breitmayer, Dominant creep mechanism and the descending lithosphere, *Geophys. J.R. Astron. Soc.* 43 (1975) 873.
- 16 S.A.F. Murrell, Rheology of the lithosphere—experimental indications, *Tectonophysics* 36 (1976) 5.
- 17 U.R. Vetter and R.O. Meissner, Creep in geodynamic processes, *Tectonophysics* 42 (1977) 37.
- 18 C. Froidevaux, G. Schubert and D.A. Yuen, Thermal and mechanical structure of the upper mantle: a comparison between continental and oceanic models, *Tectonophysics* 37 (1977) 233.
- 19 D.T. Griggs, F.J. Turner and H.C. Heard, Deformation of rocks at 500°C–800°C, in: *Rock Deformation*, *Geol. Soc. Am. Mem.* 79 (1960) 39.
- 20 C. Goetze and W.F. Brace, Laboratory observations of high-temperature rheology of rocks, *Tectonophysics* 13 (1972) 583.
- 21 R.L. Stocker and M.F. Ashby, On the rheology of the upper mantle. *Rev. Geophys. Space Phys.* 11/2 (1973) 391.
- 22 D.L. Kohlstedt and C. Goetze, Low-stress high-temperature creep in olivine single crystals, *J. Geophys. Res.* 79 (1974) 2045.
- 23 J. Weertman and J.R. Weertman, High-temperature creep of rock and mantle viscosity, *Ann. Rev. Earth Planet. Sci.* 3 (1975) 293.
- 24 D.L. Kohlstedt and C. Goetze and W.B. Durham, Experimental deformation of single crystal Olivine with application to flow in the mantle, in: *Physics and Chemistry of Rocks and Minerals* (J. Wiley and Sons, New York, N.Y., 1976).
- 25 D.L. Turcotte, D.C. McAadoo and J.G. Caldwell, An elastic-perfectly plastic analysis of the bending lithosphere, *Tectonophysics* 47 (1978) 193.
- 26 D.C. McAadoo, J.G. Caldwell and D.L. Turcotte, On the elastic-perfectly plastic bending of the lithosphere under generalized loading with application to the Kuril trench, *Geophys. J.R. Astron. Soc.*, 54 (1978) 11.
- 27 T.W.C. Hilde, N. Isezaki and J.M. Wageman, Mesozoic sea-

- floor spreading in the North Pacific, *Am. Geophys. Union Geophys. Monogr.* 19 (1976) 205.
- 28 D. Hussong and S. Cande, Mesozoic lineations in the Mariana basin (in preparation).
- 29 D.E. Hayes, C. Mrozowski and R. Jarrard, A geophysical/structural section across the IDOE/IPOD Philippine-Mariana transect zone (in preparation).
- 30 R.E. Houtz, unpublished data.
- 31 X. Le Pichon, J. Francheteau and J. Bonnin, *Plate Tectonics* (Elsevier, Amsterdam, 1976).
- 32 L.M. Kachanov, *Fundamentals of the Theory of Plasticity* (Mir Publishers, Moscow, 1974).
- 33 W. Prager and P.G. Hodge, *Theory of Perfectly Plastic Solids* (J. Wiley and Sons, New York, N.Y., 1951).
- 34 C.H. Scholz, Microfracturing and the inelastic deformation of rock in compression, *J. Geophys. Res.* 73 (1968) 1417.
- 35 K. Mogi, Fracture and flow of rocks, in: *Physics and Chemistry of Rocks and Minerals* (J. Wiley and Sons, New York, N.Y., 1976).
- 36 C. Goetze, The mechanisms of creep in Olivine, *Philos. Trans. R. Soc. London, Ser. A*, 288 (1978) 99.
- 37 C. Goetze, Stress and temperature in the bending lithosphere as constrained by experimental rock mechanisms (in preparation).
- 38 M. Barazangi and J. Dorman, World seismicity maps compiled from ESSA, Coast and Geodetic Survey, epicenter data, 1961–1067. *Bull. Seismol. Soc. Am.* 59 (1969) 369.
- 39 M. Katsumata and L.R. Sykes, Seismicity and tectonics of the western Pacific: Izu-Mariana-Caroline and Ryukyu-Taiwan regions, *J. Geophys. Res.* 74 (1969) 5923.
- 40 H. Kanamori, Seismic and aseismic slip along subduction zones and their tectonic implications, in: *Island Arcs, Deep Sea Trenches, and Back-Arc Basins*, M. Talwani and W.C. Pitman III, eds., *Am. Geophys. Union, Maurice Ewing Ser.* 1 (1976) 163.
- 41 J. Kelleher, L. Sykes and J. Oliver, Possible criteria for predicting earthquake locations and their applications to major plate boundaries of the Pacific and the Caribbean, *J. Geophys. Res.* 78 (1973) 2547.
- 42 Rev. Jose Algué, Mirador Observatory Baguio. Benquet: A New Meteorological-Geodynamic Station of the Weather Bureau (Bureau of Printing, Manila, 1909) 26–27.
- 43 D.E. Karig, Structural history of the Mariana island arc system, *Geol. Soc. Am. Bull.* 82 (1971) 323.
- 44 D.E. Karig and G.F. Moore, Tectonic complexities in the Bonin arc system, *Tectonophysics* 27 (1975) 97.
- 45 D.E. Karig, R.N. Anderson and L.D. Bibee, Characteristics of back arc spreading in the Mariana trough, *J. Geophys. Res.* 83 (1978) 1213.
- 46 H. Kanamori and K. Tsumura, Spatial distribution of earthquakes in the Kii peninsula, Japan, south of the median tectonic line, *Tectonophysics* 12 (1971) 327.
- 47 J. Kelleher and W. McCann, Buoyant zones, great earthquakes, and unstable boundaries of subduction, *J. Geophys. Res.* 81 (1976) 4885.

## Appendix. Development of an elastic-plastic varying yield stress model

We define  $y = \zeta_1$  and  $\zeta_2$  to be the upper and lower limits of the elastic portion of the plate, respectively, within regions IIA and IIB.  $\zeta_0$  is the midpoint of these limits (Fig. 3). Note, that within region IIA,  $\zeta_1$  and  $\zeta_2$  will not both be found within the thickness of the slab. Remembering that the curvature is proportional to the bending moment for purely elastic deformation, we can consider the quantity  $\zeta_1 - \zeta_2$  to be an elastic thickness associated with a curvature (and thus a bending moment  $-M_c$ ) for which the plastic yield condition has just been reached at the top and bottom of a bending plate. For a constant yield stress,  $\sigma_0$ , using (10) (neglecting horizontal loading), where  $y = (\zeta_1 - \zeta_2)/2$ , and  $H = \zeta_1 - \zeta_2$ , we get:

$$M_c = \sigma_0 \frac{(\zeta_1 - \zeta_2)^2}{6} \quad (11a)$$

For a depth-dependent yield stress,  $\sigma_1 + \sigma_2 y$  (where  $\sigma_1$  = yield stress found at  $y = 0$ , and  $\sigma_2$  = yield stress gradient), using equation (10) we get:

$$M_c = \frac{(\sigma_1 + \sigma_2 \zeta_0)}{6} (\zeta_1 - \zeta_2)^2 \quad (11b)$$

The curvature is then related to the stress distribution using equation (4) letting  $D = E(\zeta_1 - \zeta_2)^3/12(1 - \nu^2)$  to find:

$$\frac{d^2 w}{dx^2} = \frac{-2\sigma_0(1 - \nu^2)}{E(\zeta_1 - \zeta_2)} \quad (12)$$

for constant yield stress, and:

$$\frac{d^2w}{dx^2} = \frac{-2(\sigma_1 + \sigma_2 \zeta_0)(1 - \nu^2)}{E(\zeta_1 - \zeta_2)} \quad (13)$$

for depth-dependent yield stress. We see that the expressions for the two rheologies become equivalent as  $\sigma_2 \rightarrow 0$ . We thus continue developing only the depth-dependent yield stress model.

We next find expressions for  $\zeta_1 - \zeta_2$  and  $\zeta_0$  by integrating (9) and (10) across the stress profile (14), solving for  $T(\zeta_1, \zeta_2)$  and  $M(\zeta_1, \zeta_2)$ .

$$\sigma_x(y) = \begin{cases} \sigma_1 + \sigma_2 y & \zeta_1 \leq y \leq H/2 \\ \frac{2}{\zeta_1 - \zeta_2} [y(\sigma_1 + \sigma_2 \zeta_0) - \sigma_1 \zeta_0 - \sigma_2 \zeta_1 \zeta_2] & \zeta_2 \leq y \leq \zeta_1 \\ -(\sigma_1 + \sigma_2 y) & -H/2 \leq y \leq \zeta_2 \end{cases} \quad (14)$$

to find, for region IIA:

$$T = \frac{1}{\zeta_0 - \zeta_i} \left[ (\sigma_1 + \sigma_2 \zeta_k) \left( \frac{H^2}{8} + \frac{\zeta_i^2}{2} \right) - \frac{\zeta_0 - \zeta_i}{|\zeta_0 - \zeta_i|} (\sigma_1 + \sigma_2 \zeta_i) \frac{\zeta_k H}{2} \right] \quad (15)$$

$$M = \frac{1}{\zeta_0 - \zeta_i} \left[ (\sigma_1 + \sigma_2 \zeta_k) \left( \frac{\zeta_i^3}{6} - \frac{H^2 \zeta_i}{8} \right) + \frac{\zeta_0 - \zeta_i}{|\zeta_0 - \zeta_i|} (\sigma_1 + \sigma_2 \zeta_i) \frac{H^3}{24} \right] \quad (16)$$

where:

$i = 1 \quad k = 2$  top of plate yields first

$i = 2 \quad k = 1$  bottom of plate yields first

and region IIB:

$$T = -\sigma_1(\zeta_1 + \zeta_2) + \sigma_2 \left( \frac{H^2}{4} - \zeta_1 \zeta_2 \right) \quad (17)$$

$$M = \frac{\sigma_1 H^2}{4} - \frac{\sigma_1}{4} (\zeta_1 + \zeta_2)^2 - \frac{\sigma_1}{12} (\zeta_1 - \zeta_2)^2 - \frac{\sigma_2}{3} \zeta_1 \zeta_2 (\zeta_1 + \zeta_2) \quad (18)$$

To solve (13) in each region we must find  $\zeta_1 - \zeta_2$  and  $\zeta_0$ . To simplify, we let  $\sigma_1 H^2/4 = XM_1$ ,  $\sigma_2 H^2/4 = XM_2$ ,  $\sigma_1 H = T_1$ ,  $\sigma_2 H = T_2$ .

For region IIA we combine (15) and (16) to eliminate  $\zeta_k$ . The result is a fourth-order polynomial in  $\zeta_1$  or  $\zeta_2$  which must be solved for the correct root. For yielding at the top of the plate first:

$$\begin{aligned} & (T\sigma_2 - T_2\sigma_1)\zeta_1^4 + [\sigma_1(T - T_1 - 4XM_2) - \sigma_2(3M - 4XM_1 - XM_2H)]\zeta_1^3 + [(4XM_1 - 3M + XM_2H)T_2 \\ & - 3\sigma_1M - 3TXM_2]\zeta_1^2 + [(T - T_1)(-XM_2H - 3XM_1) - 3M(T_1 + XM_2) + T_2XM_1H + H(XM_2)^2]\zeta_1 \\ & + XM_1[(T_1 - T + XM_2)H - 3M] = 0 \end{aligned} \quad (19)$$

For yielding at the bottom first:

$$\begin{aligned} & (T\sigma_2 + T_2\sigma_1)\zeta_2^4 + [\sigma_1(T + T_1 - 4XM_2) - \sigma_2(3M - 4XM_1 + XM_2H)]\zeta_2^3 + [(-4XM_1 + 3M + XM_2H)T_2 \\ & - 3\sigma_1M - 3TXM_2]\zeta_2^2 + [(T + T_1)(XM_2H - 3XM_1) - 3M(-T_1 + XM_2) + T_2XM_1H - H(XM_2)^2]\zeta_2 \\ & + XM_1[(T + T_1 - XM_2)H - 3M] = 0 \end{aligned} \quad (20)$$

$\zeta_1 - \zeta_2$  and  $\zeta_0$  are computed from the solution of (19) or (20) and substitution back into the expression for  $T$  or

$M$ . The solutions for  $\zeta_1 - \zeta_2$  and  $\zeta_0$  are derived in a similar fashion for region IIB by solving for  $\zeta_2$  from

$$[\sigma_2(XM_2 - T) + \sigma_1^2]\zeta_2^2 + [\sigma_1(T - XM_2) + 3\sigma_2(M - XM_1)]\zeta_2 + [3\sigma_1(M - XM_1) + (T - XM_2)^2] = 0 \quad (21)$$

Equilibrium equations (1) to (3) can be combined to give:

$$\frac{d^2M}{dx^2} = -T \frac{d^2w}{dx^2} + kw \quad (22)$$

Using (22), (13) and the appropriate solutions for  $\zeta_1 - \zeta_2$  and  $\zeta_0$  for regions IIA and IIB, we solve for the deflection by means of a fourth-order Runge-Kutta algorithm with stepwise integration through region II from the elastic region I. As described in McAdoo et al. [26], this procedure is only valid until region III is reached where the bending moment reaches a maximum and unbending begins. Although at this point plastic yielding ceases and the plate is again entirely elastic, the stress distribution through the plate is partly determined by the previous inelastic deformation and is non-linear. The deflections in this region may be approximated by integrating (1) to (3) and:

$$\frac{d^3w}{dx^3} = -\frac{1}{D} \frac{dM}{dx} \quad (23)$$